UC San Diego

UC San Diego Electronic Theses and Dissertations

Title

The role of labile iron in macrophage proinflammatory activation.

Permalink

https://escholarship.org/uc/item/4pp8m9hz

Author

Farrell, Andrea Araceli

Publication Date

2024

Peer reviewed|Thesis/dissertation

eScholarship.org Powered by the California Digital Library
University of California

UNIVERSITY OF CALIFORNIA SAN DIEGO

The role of labile iron in macrophage proinflammatory activation.

A Thesis submitted in partial satisfaction of the requirements
for the degree Master of Science

in

Biology

by

Andrea Farrell

Committee in charge:

Professor Wei Ying, Chair
Professor Enfu Hui, Co-Chair
Professor Scott Biering

2024

Copyright

Andrea Farrell, 2024

All rights reserved.

The Thesis of Andrea Farrell is approved, and it is acceptable in quality and form for publication on microfilm and electronically.

University of California San Diego

2024

TABLE OF CONTENTS

THESIS APPROVAL PAGE iii

TABLE OF CONTENTS iv

LIST OF FIGURES v

ACKNOWLEDGEMENTS vi

ABSTRACT OF THE THESIS vii

INTRODUCTION 1

Chapter 1 RESULTS 3

Chapter 2 DISCUSSION 18

Chapter 3 MATERIALS AND METHODS 21

REFERENCES 25

LIST OF FIGURES

Figure 1: Iron phenotypes in bone marrow derived macrophages (BMDMs) in response to LPS. 4

Figure 2: LPS induces labile iron deficiency in BMDMs.. 5

Figure 3: Effect of iron supplementation on BMDM proinflammatory responses. 6

Figure 4: Effect of iron chelator on BMDM proinflammatory response 7

Figure 5: Mitochondrial phenotypes in BMDMs when challenged with LPS. 8

Figure 6: Effect of Ncoa4 mutation on BMDM iron homeostasis 9

Figure 7: Effects of Ncoa4 mutation on iron phenotypes of BMDMs 10

Figure 8: Hepatic macrophage phenotypes after LPS injection 11

Figure 9: Effect of LPS on labile iron pool of emKCs. emKC labile iron pool 12

Figure 10: Iron phenotypes in RHMs and KC-like cells in response to LPS 13

Figure 11: Effect of MyD88 depletion on the proinflammatory responses of emKCs and RHMs 14

Figure 12: Effects of Fth knockout on emKC phenotypes in response to LPS. 16

Figure 13: emKC phenotypes after 2 weeks of LPS injection. 17

ACKNOWLEDGEMENTS

I would like to acknowledge Professor Wei Ying for their support and guidance as my faculty advisor. I would also like to thank Ke Wang, Ph.D., and Karina Cunha e Rocha, Ph.D. for training me in the necessary laboratory techniques, and the members of the Ying lab for their support throughout the project.

ABSTRACT OF THE THESIS

The role of labile iron in macrophage proinflammatory activation.

by

Andrea Farrell

Master of Science in Biology

University of California San Diego, 2024

Professor Wei Ying, Chair
Professor Enfu Hui, Co-Chair

Iron is found within the cell as Fe^{3+}, ferritin-bound iron, and Fe^{2+}, intracellular labile iron, which can be readily used for a variety of cellular functions, especially in the mitochondria. Macrophages, a major site for iron storage and recycling, undergo significant metabolic changes upon activation. Here, we demonstrate that sequestration of the labile iron pool to the mitochondria is characteristic of the macrophage proinflammatory response. Using LPS to stimulate proinflammatory activation in bone marrow derived macrophage (BMDMs)

and embryonic Kupffer cells (emKCs), we measured labile iron content and mitochondrial iron with specific probes detected by flow cytometry. The expression of key iron metabolism genes and proinflammatory cytokines were measured to assess the iron metabolism and proinflammatory responses of macrophages. Treatment with LPS *in vitro* and *in vivo* demonstrated increased the mitochondrial Fe^{2+} content, while the intracellular labile iron pool was decreased. The emKC population was decreased after LPS stimulation, but this effect was attenuated by depletion of ferritin. Other hepatic macrophage populations, Kupffer cell-like (KC-like) cells and recruited hepatic macrophages (RHMs), increased in response to LPS. *Nrf2*, a master regulator of redox homeostasis, which was repressed in emKCs but upregulated in KC-like cells and RHMs, may be key to understanding the differences in responses to LPS exhibited by these macrophage populations. Our results expand upon the interplay between iron homeostasis and the metabolic changes required for macrophage activation.

INTRODUCTION

Metabolic plasticity is critical to initiating specific functions in macrophages in response to distinct stimuli[1-3]. Early studies have shown that, at the early stage (the first 2 hours) of lipopolysaccharide (LPS) stimulation, the activation of TLR4 signaling of bone marrow-derived macrophages (BMDMs) quickly promotes glycolysis and tricarboxylic acid cycle volume, which elevate the levels of acetyl-Coenzyme A and histone activation, leading to expression of proinflammatory genes[3]. At the late stage (>12 hours) of LPS treatment, BMDMs are characterized by repressed mitochondrial activities[3].

Iron is an essential nutrient involved in many aspects of cell metabolism. Intracellular iron is found in labile iron pools as redox-active Fe^{2+} and is stored in ferritin as ferric iron [4, 5]. NCOA4 (nuclear receptor coactivator 4) can bind ferritin and mediate its autophagic degradation to release ferritin-bound iron for cellular use[6-8]. Macrophages are iron-enriched cells, and they recycle iron by phagocytosis of erythrocytes. They export iron via ferroportin (*Fpn*) and import iron via transferrin receptor (*Tfrc1*)[9-12]. Previous studies have shown that either iron deficiency or overload result in abnormal macrophage functions[13-15]. While labile iron is essential for various biological activities, including mitochondrial functions[4, 16-18], how labile iron influx contributes to the metabolic changes during macrophage activation is still largely unknown.

The liver is a major site for iron storage and plays an important role in filtering bacteria and bacterial components from the circulation. The ability of the liver to remove bacterial components from the bloodstream is mainly attributed to the phagocytosis function of embryonic Kupffer cells (emKCs). Loss of emKCs, such as in obesity, results in the accumulation of bacterial DNA in host tissues[19, 20]. emKCs are iron-enriched cells that are crucial for iron

recycling[9]. Yet, little is known about how labile iron levels could be adjusted in emKCs after proinflammatory response to bacterial components.

Here, we report that, in both *in vitro* and *in vivo* experiments, an increase in labile iron influx from the labile iron pool to the mitochondria occurs in macrophages when initiating LPS-induced proinflammatory activation. Enhancing mitochondrial Fe^{2+} content promotes proinflammatory cytokine expression in response to LPS. LPS-treated BMDMs are iron deficient, while more ferritin-bound iron is observed in emKCs after LPS challenging. LPS-induced iron overload also occurs in KC-like cells and recruited hepatic macrophages (RHMs). Additionally, emKC loss is observed after LPS treatment. Unlike emKCs, the population of KC-like cells and RHMs increased in LPS-injected mice. The activation of MyD88-mediated cascade signaling also exerts profound regulation on the expression of iron metabolism key genes.

Chapter 1 RESULTS

Macrophage iron mobilization in response to proinflammatory activation.

We first examined the iron phenotypes in bone marrow-derived macrophages (BMDMs) prepared from 10-12wks old male B6/C57 WT mice[21]. Given that BMDMs display distinct mitochondrial activities at early (<8 hours) vs. late stage (>12 hours) of LPS stimulation[3], we analyzed the status of iron metabolism of BMDMs after 2 hours or 24 hours of LPS treatment (10ng/ml). As shown in **Figures 1A-C**, the abundance of iron metabolism key genes, including ferritin (*Fth1*; iron storing protein)[5], transferrin receptor (*Tfrc1*; iron importer)[22], and ferroprotein (*Fpn*; iron exporter)[10-12], were quickly decreased after 2 hours of LPS stimulation, indicating iron deficiency in BMDMs. Consistent with previous reports[3, 23], the expression of proinflammatory cytokines, including *Il1b*, *Tnfa*, *Cxcl1*, and *Il12b*, was markedly increased in BMDMs after 2 hours of LPS stimulation (**Figures 1D-G**). 24 hours of LPS treatment further repressed the expression of iron metabolism key genes, but the LPS-induced surge in the expression of *Il1b*, *Tnfa*, *Cxcl1*, and *Il12b* was attenuated after 24 hours (**Figures 1A-G)**. We also observed similar phenotypes of iron deficiency from LPS-treated BMDMs prepared from 10-12wks female B6/C57 WT mice (**Figures 1H-J**).

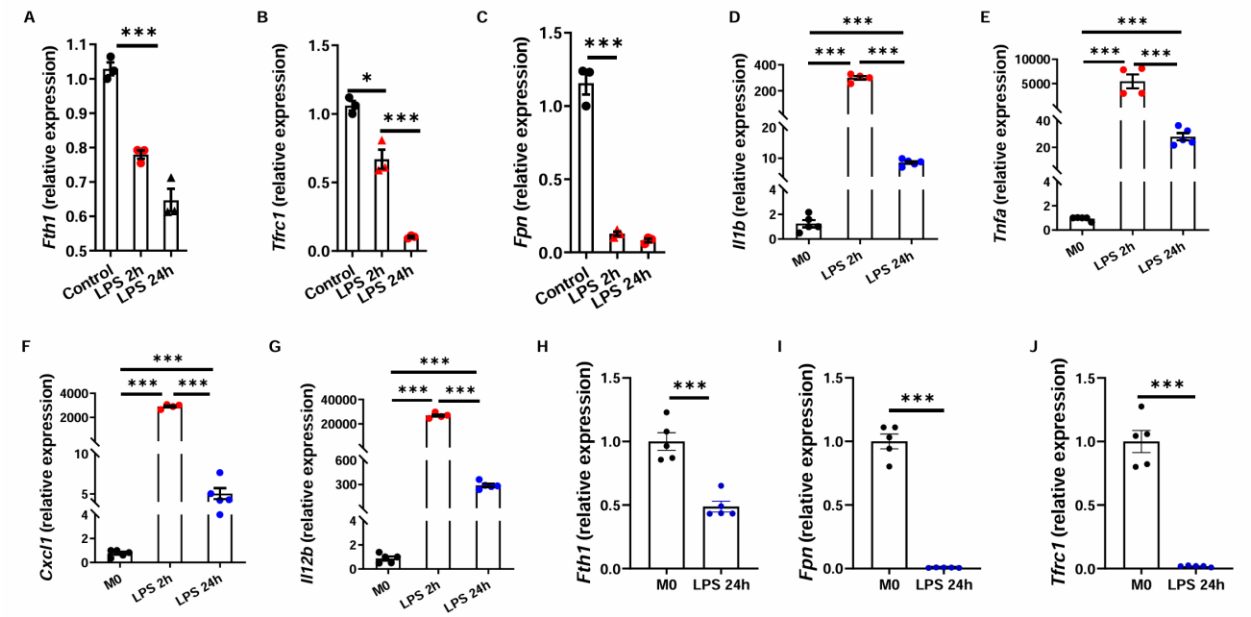


Figure 1: Iron phenotypes in bone marrow derived macrophages (BMDMs) in response to LPS. The expression of *Fth1* (A), *Tfrc1* (B), and *Fpn* (C) in BMDMs after 2 or 24 hours of LPS treatment. The abundance of proinflammatory cytokines *Il1b* (D), *Tnfa* (E), *Cxcl1* (F), and *Il12b* (G) in BMDMs after 2 or 24 hours of LPS treatment. Effect of LPS on the expression of *Fth1* (H), *Fpn* (I), and *Tfrc1* (J) in female BMDMs. Data are presented as mean ± SEM. **P* < 0.05, ***P* < 0.01, ****P* < 0.001, Student's t-test.

Given that LPS treatment tunes down iron metabolism activities in BMDMs, we further evaluated the impact of LPS on the levels of the labile iron pool, which mainly localizes inside the endoplasmic reticulum (ER) and plays critical roles in various biological activities such as mitochondrial functions[4, 16-18]. A labile iron fluorescent probe that only reacts with ER-bound Fe^{2+} and irreversibly turns it into a far-red fluorescent subtract was used to measure the abundance of labile iron[24]. Interestingly, the levels of labile iron pool were significantly decreased after LPS challenging (**Figure 2A**). In contrast, the levels of labile iron pool were not significantly changed in BMDMs after 24 hours of IL4/IL13 (20ng/ml) treatment (**Figure 2B**). Consistent with labile iron deficiency in LPS-treated BMDMs, we found that *Ncoa4*, the key mediator producing labile iron from ferritinophagy[6-8], was remarkably decreased in the presence

of LPS (**Figures 2C&D**). IL4/IL13 stimulation had minimal effects on *Ncoa4* expression in BMDMs (**Figures 2C)**. Thus, these data indicate that male BMDMs are labile iron deficient when challenged with LPS.

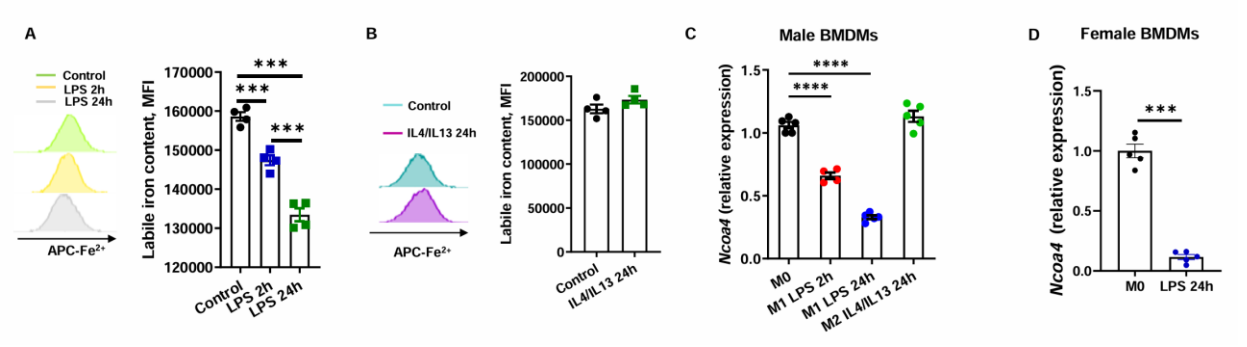


Figure 2: LPS induces labile iron deficiency in BMDMs. (A) The levels of labile iron pool in BMDMs after 2 or 24 hours of LPS treatment. (B) Effect of IL4/IL13 on BMDM labile iron pool. (C) *Ncoa4* abundance in BMDMs in response to either LPS or IL4/IL13 stimulation. (D) *Ncoa4* expression in female BMDMs in response to LPS treatment. Data are presented as mean ± SEM. **P* < 0.05, ***P* < 0.01, ****P* < 0.001, Student's t-test.

LPS-induced reduction in *Fth1* abundance indicates iron deficiency in BMDMs[4]. Hence, we evaluated whether replenishing iron levels could affect macrophage proinflammatory responses. BMDMs were treated with FAC (ferric ammonium citrate; 100nM) to supplement iron. In naïve BMDMs, 24 hours of FAC treatment increased intracellular iron content, as evidenced by increased abundance of *Fth1* in BMDMs (**Figure 3A**). In addition, FAC-treated BMDMs increased the expression of iron exporter *Fpn* and labile iron pool regulator *Ncoa4* and tuned down iron importer *Tfrc1* levels to re-balance iron homeostasis (**Figures 3B-C**). In naïve BMDMs, FAC treatment did not trigger proinflammatory cytokine production (**Figures 3E-G**). When co-treated with LPS and FAC, the expression of the key genes associated with iron metabolism was still remarkably down-regulated to the levels observed in BMDMs treated with LPS alone (**Figures 3A-D**). In contrast, FAC co-treatment resulted in greater levels of iron supply, as shown by greater expression of *Fth* and *Ncoa4* than cells treated with LPS alone

(**Figures 3A-D**). Additionally, FAC treatment elevated the expression of proinflammatory cytokines *Il1b*, *Tnfa*, and *Il12b* in BMDMs in response to LPS stimulation (**Figures 3E-G**).

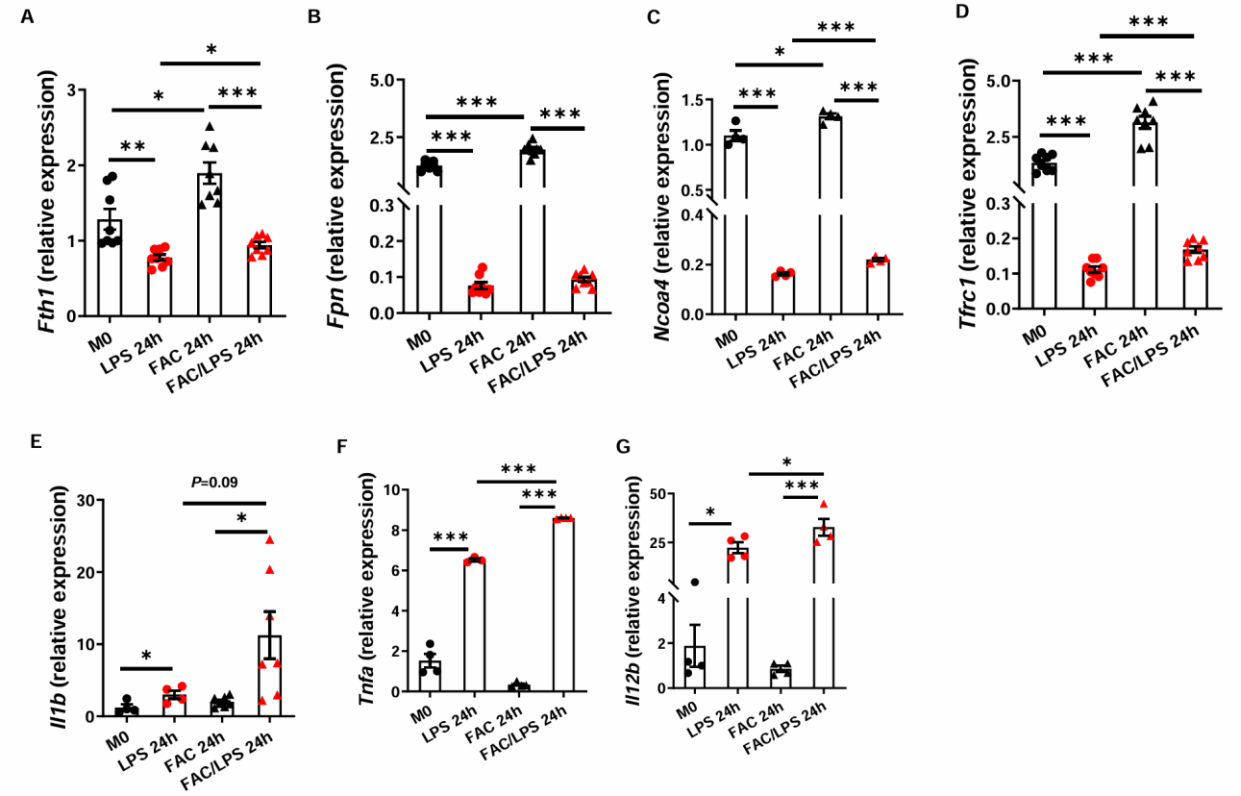


Figure 3: Effect of iron supplementation on BMDM proinflammatory responses. The expression of *Fth1* (A), *Fpn* (B), *Ncoa4* (C), and *Tfrc1* (D) in BMDMs in the presence of LPS and/or FAC. The abundance of proinflammatory cytokines *Il1b* (E), *Tnfa* (F), and *Il12b* in BMDMs when treated with LPS and/or FAC. Data are presented as mean ± SEM. **P* < 0.05, ***P* < 0.01, ****P* < 0.001, Student's t-test.

Most iron is Fe^{3+} (ferric iron) that is bound with ferritin, and it can be released and converted to Fe^{2+} that is an active form required for various biological activities. We also assess the effect of iron deficiency on macrophage proinflammatory activation. Naïve BMDMs were treated with an iron chelator, deferoxamine (DFO; 100µM), which efficiently chelates Fe3+[25]. After 24 hours, DFO treatment had minimal effects on proinflammatory cytokine production (**Figures 4A-C**). DFO-pretreated BMDMs also had comparable abundance of LPS-induced proinflammatory cytokines as that in BMDMs treated with only LPS (**Figures 4A-C**). Previous

studies reported that DFO has low membrane permeability in some cell types[26]. As shown in **Figure 4D**, *Fth1*, the indicator of cellular iron mass, was not changed by DFO treatment in BMDMs. In addition, DFO treatment did not affect the expression of other key genes associated with iron metabolism (**Figures 4E-G**). Thus, DFO failed to chelate iron in BMDMs.

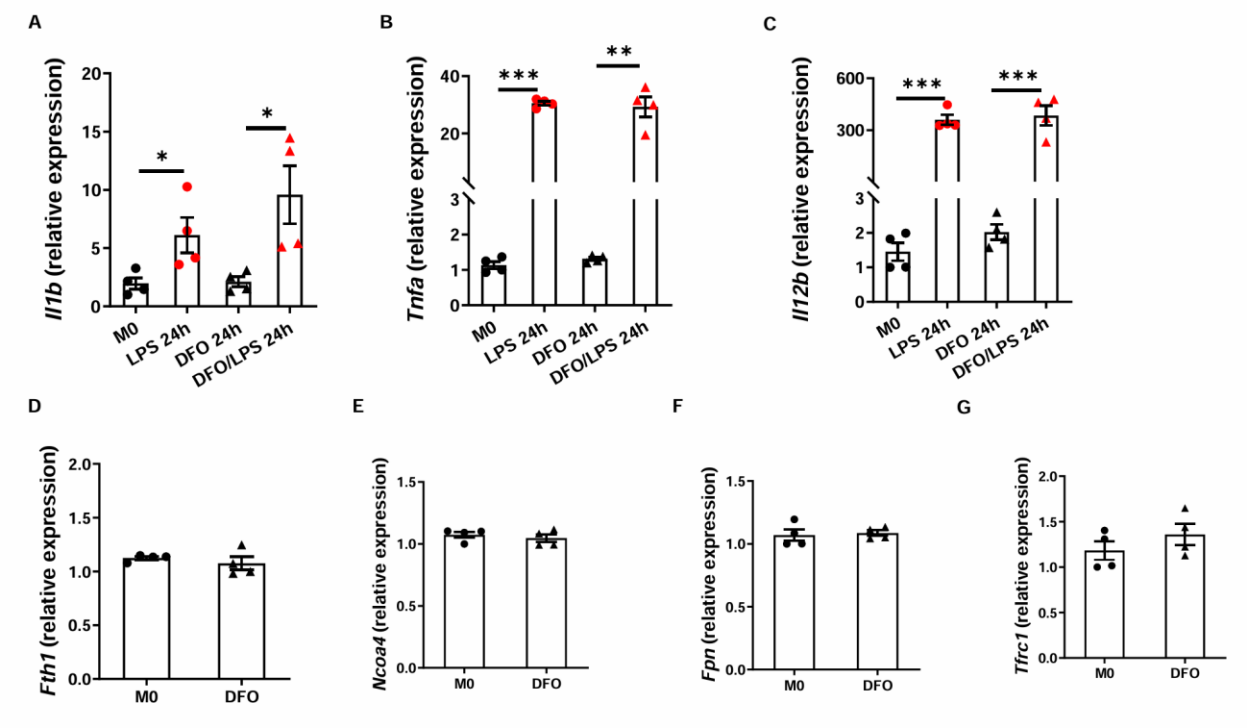


Figure 4: Effect of iron chelator on BMDM proinflammatory responses. The expression of *Il1b* (A), *Tnfa* (B), and *Il12b* (C) in DFO-pretreated BMDMs in response to LPS. The abundance of *Fth1* (D), *Ncoa4* (E), *Fpn* (F) and *Tfrc1* (G) in BMDMs when treated with DFO. Data are presented as mean ± SEM. **P* < 0.05, ***P* < 0.01, ****P* < 0.001, Student's t-test.

Mitochondrial iron content is elevated in response to proinflammatory activation.

Labile iron is essential for mitochondrial functions, which are required for an acute proinflammatory activation in macrophages[4, 16-18], We next examined mitochondrial phenotypes in BMDMs in response to LPS stimulation. We used flow cytometric analysis with a fluorescent probe (Mito-FerroGreen) to specifically detect mitochondrial Fe^{2+} which are mainly bound in Fe-S clusters and heme proteins within mitochondria[9, 27]. In contrast to the rapid reduction in labile

iron pool, mitochondrial Fe^{2+} levels were quickly elevated in BMDMs after 2 hours of LPS stimulation (**Figure 5A**). While previous studies have shown that BMDMs had increased mitochondrial activities during the early stage of LPS stimulation[3], BMDM mitochondrial mass and ROS levels were not significantly changed after 2 hours of LPS treatment, as measured by MitoTrack Green and MitoSOX probes, respectively (**Figures 5B&C**)[28, 29]. We also observed the increase in mitochondrial Fe^{2+} content was maintained after 24 hours of LPS stimulation (**Figure 5A**). However, both MitoTrack Green and MitoSOX probe signal intensities were decreased in 24 hour-LPS stimulated BMDMs compared to M0 BMDMs (**Figures 5B&C**), suggesting a suppression on mitochondrial activities after prolonged LPS stimulation.

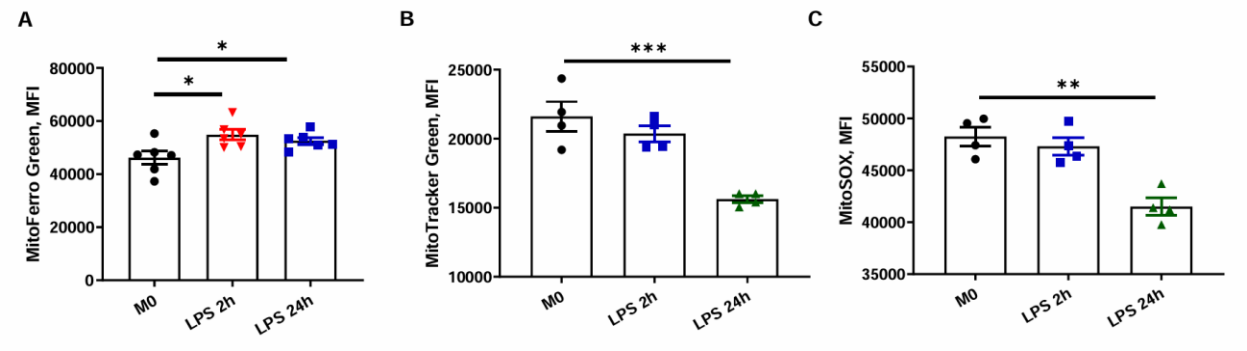


Figure 5: Mitochondrial phenotypes in BMDMs when challenged with LPS. After 2 or 24 hours of LPS treatment, the levels of mitochondrial Fe2+ content, mass, and ROS in BMDMs measured by MitoFerro Green (A), MitoTracker Green (B), or MitoSOX (C) probe, respectively. Data are presented as mean ± SEM. *$P < 0.05$, **$P < 0.01$, ***$P < 0.001$, Student's t-test.

NCOA4 depletion has minimal effects on BMDM proinflammatory activation.

Given that NCOA4 plays a critical role in mediating labile iron pool, we first examined the role of *Ncoa4* in macrophage development by transfection of siRNA-Ncoa4 (10pmol/1x10^6 cells) when seeding bone marrow cells. After 7 days, siRNA-Ncoa4 transfection led to about 60% reduction in *Ncoa4* abundance, compared to the control cells transfected with scramble siRNA (**Figure 6A**). As shown in **Figures 6B&C**, *Ncoa4* repression had minimal effects on

macrophage maturation, as evidenced by comparable levels of F4/80 abundance and CD11b^{high}F4/80^{high} population between cells transfected with either siRNA-Ncoa4 or scramble siRNA. In addition, the levels of labile iron pool, mitochondrial Fe^{2+}, and mitochondrial mass were not affected when mutating *Ncoa4* during macrophage differentiation (**Figures 6C-F**).

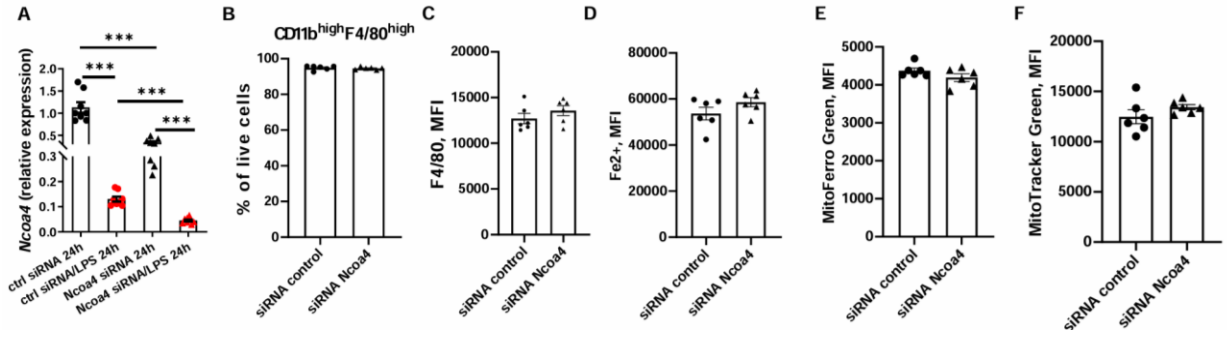


Figure 6: Effect of *Ncoa4* mutation on BMDM iron homeostasis. (A) *Ncoa4* depletion in BMDMs by transfection of siRNA-Ncoa4. Control cells were transfected with scramble siRNA. Effect of *Ncoa4* mutation on BMDM maturation by measuring the population of CD11b^{high}F4/80^{high} cells (B) and F4/80 intensity (C). The levels of labile iron pool (D), mitochondrial Fe^{2+} (E), and mitochondrial mass (F) in WT vs Ncoa4 KO BMDMs. Data are presented as mean ± SEM. **P* < 0.05, ***P* < 0.01, ****P* < 0.001, Student's t-test.

Given that Ncoa4 was quickly reduced in BMDMs after 2 hours of LPS stimulation, we further examined the importance of Ncoa4 repression on BMDM proinflammatory activation. After 7 days macrophage differentiation, BMDMs were transfected with siRNA-Ncoa4 to deplete *Ncoa4* (Ncoa4 KO; **Figure 6A**). Control BMDMs were transfected with scramble siRNA. After 24 hours of siRNA transfection, Ncoa4 KO naïve BMDMs showed increased levels of iron metabolism, as evidenced by elevated abundance of *Fth1*, *Fpn*, and *Tfrc1* (**Figures 7A-C**). In addition, labile iron pool levels of Ncoa4 KO BMDMs were greater than that in control BMDMs (**Figure 7D**). The levels of proinflammatory cytokines were also maintained at basal levels (**Figures 7E-G**). In another set of BMDM experiments, LPS was added to the culture media of both Ncoa4 KO and control BMDMs. After 24 hours of LPS stimulation, in

control BMDMs, the expression of the key genes associated with iron metabolism was consistently repressed (**Figures 7A-C**). LPS further decreased *Ncoa4* abundance in siRNA-Ncoa4 transfected BMDMs, but not differences in the abundance of *Fpn*, *Fth1*, and *Tfrc1* between LPS-treated Ncoa4 KO and control cells (**Figures 6A&7A-C**). In addition, the labile iron pool and mitochondrial phenotypes were comparable between Ncoa4 KO and control BMDMs after 24 hours of LPS stimulation (**Figures 7D-F**). We also didn't observe significant differences in proinflammatory cytokine production among these LPS-treated BMDMs (**Figures 7G-I**). These data suggest that Ncoa4 repression may have minimal effects on proinflammatory activation of BMDMs.

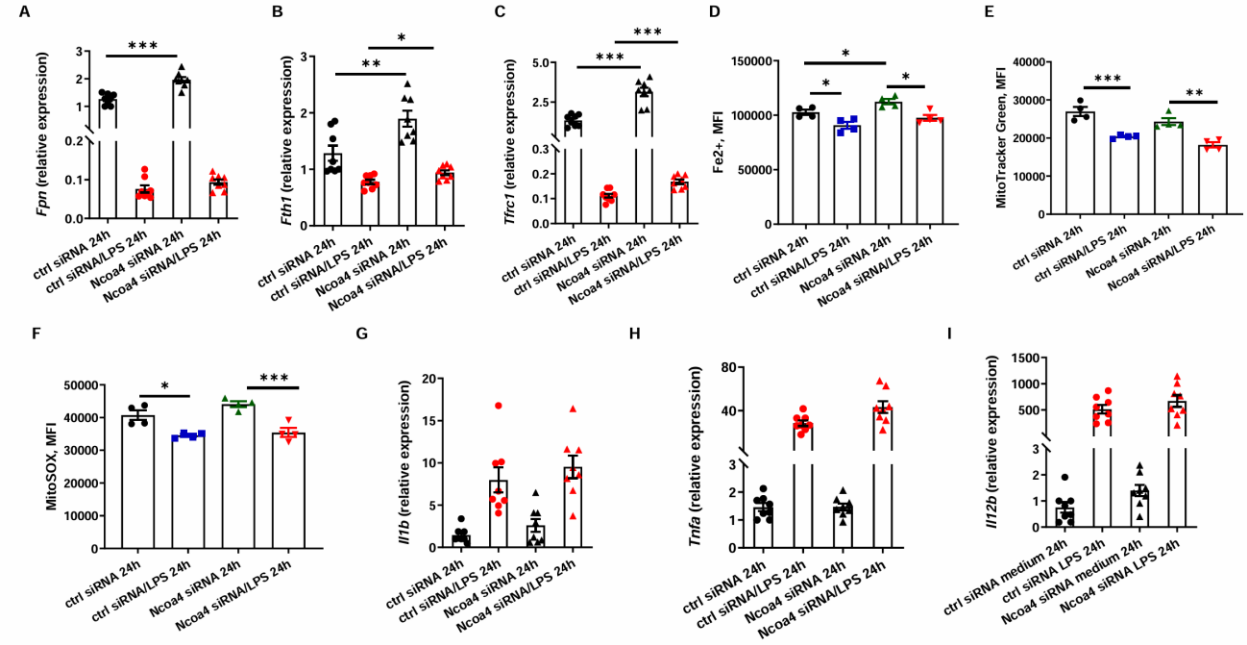


Figure 7: Effects of *Ncoa4* mutation on iron phenotypes of BMDMs. (A-C) The expression of iron metabolism key genes in Ncoa4KO (siRNA-Ncoa4) or WT (scramble siRNA) BMDMs after 24 hours of LPS treatment. The levels of labile iron pool (D) and mitochondrial mass (E) and ROS production (F) in Ncoa4KO or WT BMDMs after 24 hours of LPS treatment. The expression of proinflammatory cytokines *Il1b* (G), *Tnfa* (H), and *Il12b* (I) in Ncoa4KO or WT BMDMs after 24 hours of LPS treatment. Data are presented as mean ± SEM. **P* < 0.05, ***P* < 0.01, ****P* < 0.001, Student's t-test.

LPS causes labile iron deficiency in embryonic Kupffer cells (emKCs).

Given the marked changes in iron metabolism in BMDMs, we further assessed the iron phenotypes of tissue-resident macrophages when proinflammatory activation initiates. Bacterial infection triggers host inflammatory responses[30]. The liver plays a critical role in filtering bacteria and their byproducts when they arrive from the intestine through portal circulation. The ability of liver to remove bacterial components from the bloodstream is mainly attributed to the phagocytosis function of emKCs. Therefore, in our *in vivo* studies, mice were tail vein injected with LPS to induce proinflammatory activation of hepatic macrophages.

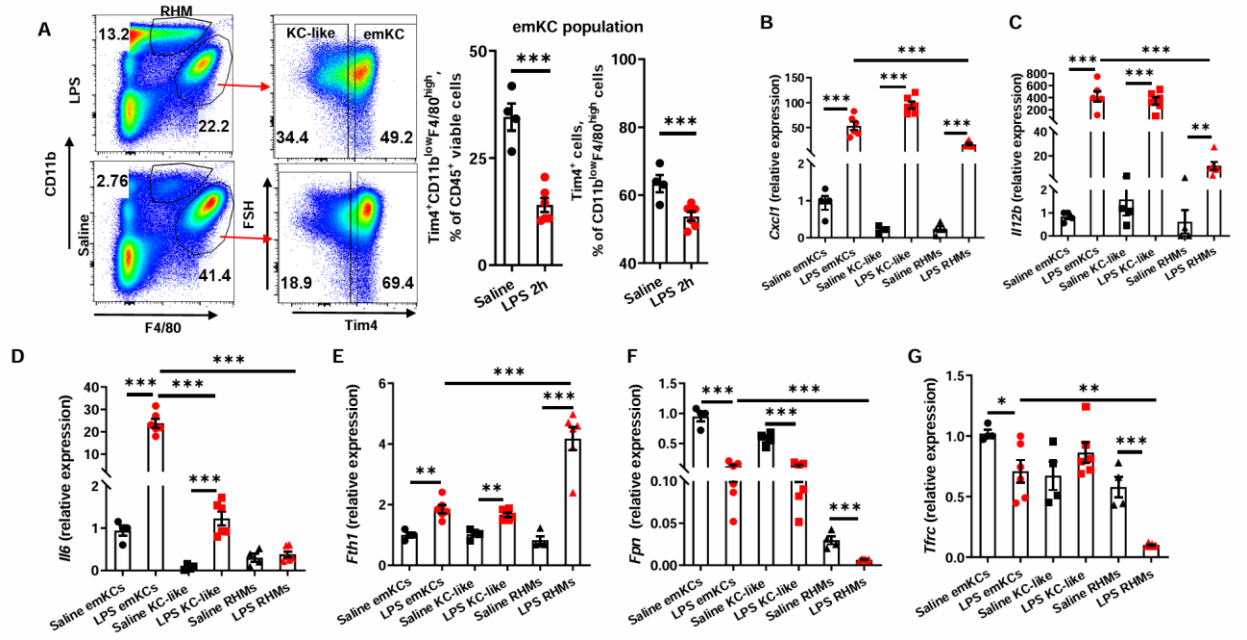


Figure 8: Hepatic macrophage phenotypes after LPS injection. After 2 hours tail-vein injection of LPS, emKC population (A; TIM4^{+}CD11b^{low}F4/80^{high}), proinflammatory gene expression (B-D), and iron metabolism gene expression (E-G) in in hepatic macrophages (KC-like cells=Tim4^{-} Clec4f+CD11b^{low}F4/80^{high}, RHM=CD11b^{high}F4/80^{low}) of normal chow diet (NCD)-fed WT mice. Data are presented as mean ± SEM. **P* < 0.05, ***P* < 0.01, ****P* < 0.001, Student's t-test.

To assess whether LPS could quickly affect hepatic macrophage responses, 10-12 weeks (wks) old lean normal chow diet (NCD) WT mice were tail vein injected with LPS (100ng per g of body weight) for 2 hours. Control mice were tail vein injected with saline. As shown in

Figure 8A, about 50% of emKCs (TIM4^{+}CD11b^{low}F4/80^{high}) were lost after 2-hour LPS injection. LPS remarkably elevated the abundance of proinflammatory genes in emKCs (**Figures 8B-D**). Interestingly, we found that the iron handling activities were greatly changed in emKCs after 2 hours of LPS injection, as shown by increased abundance of *Fth1* and repression on *Fpn* and *Tfrc1* (**Figures 8E-G**). Consistent with elevated ferritin abundance shown in **Figure 8E**, 2 hours of LPS injection caused about 50% loss in labile iron pool content in emKCs (**Figure 9A**). Consistently, the expression of *Ncoa4*, the key mediator producing labile iron from ferritinophagy[6-8], was markedly downregulated in emKCs after 2 hours of LPS injection (**Figure 9B**). As shown in **Figure 9C**, LPS induces an increase in mitochondrial Fe^{2+} levels in emKCs. However, emKC mitochondrial mass was comparable between control and LPS-injected mice (**Figure 9D**).

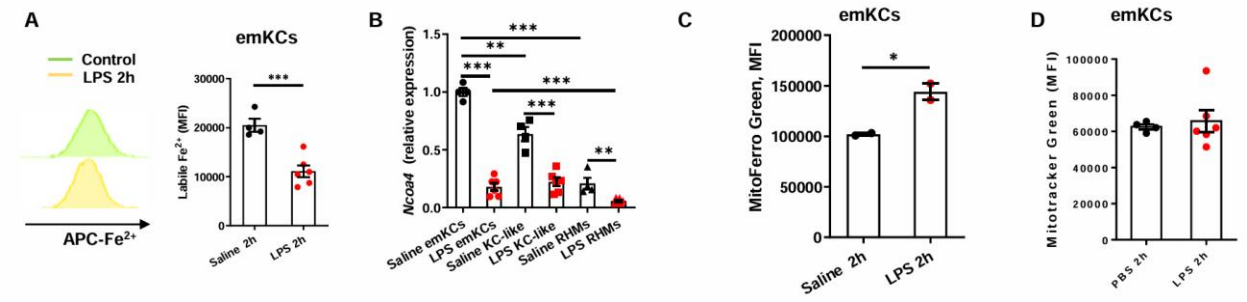


Figure 9: Effect of LPS on labile iron pool of emKCs. emKC labile iron pool (A), *Ncoa4* expression (B), mitochondrial Fe^{2+} content (C), and the abundance of mitochondria (D) after 2 hours tail-vein injection of LPS. Data are presented as mean ± SEM. $^{**}P < 0.01$, $^{***}P < 0.001$, Student's t-test.

Iron phenotypes in KC-like cells and recruited hepatic macrophages in response to LPS stimulation.

Compared to emKCs, recruited hepatic macrophages (RHMs; CD11b^{high}F4/80^{low}) harbored less labile iron (**Figures 9A vs. 10A**). While LPS-induced labile iron deficiency occurred in RHMs, the proportion of RHMs was elevated in LPS-injected mice (**Figures 10A&B**). Previous studies have indicated that a portion of RHMs became KC-like cells (TIM4^{-}

CD11b^{low}F4/80^{high})[31]. In healthy lean WT mice, KC-like cells contained lower levels of labile iron pool than emKCs (**Figures 9A vs. 10C**). After 2 hours of LPS injection, KC-like cell population was significantly increased and also exhibited reduction in labile iron pool (**Figures 10C&D**). Similar to emKCs, the repression of *Fpn* and *Ncoa4* abundance and an increase in ferritin were also found in RHMs and KC-like cells after 2 hours of LPS treatment (**Figures 8E&F, 9B**). In addition, *Tfrc1* expression was greatly decreased in RHMs, but not KC-like cells (**Figure 8G**). However, the expression of *Nrf2*, a master regulator of redox homeostasis[32, 33], was elevated in RHMs and KC-like cells, but downregulated in emKCs, in response to LPS treatment (**Figure 10E**). In addition, we found that RHMs expressed a much lower abundance of *Cxcl1*, *Il12b*, and *Il1b* than emKCs in the presence of LPS, and KC-like cells had similar levels of LPS-induced *Il12b* and *Tnfa* to emKCs (**Figure 8B-D**).

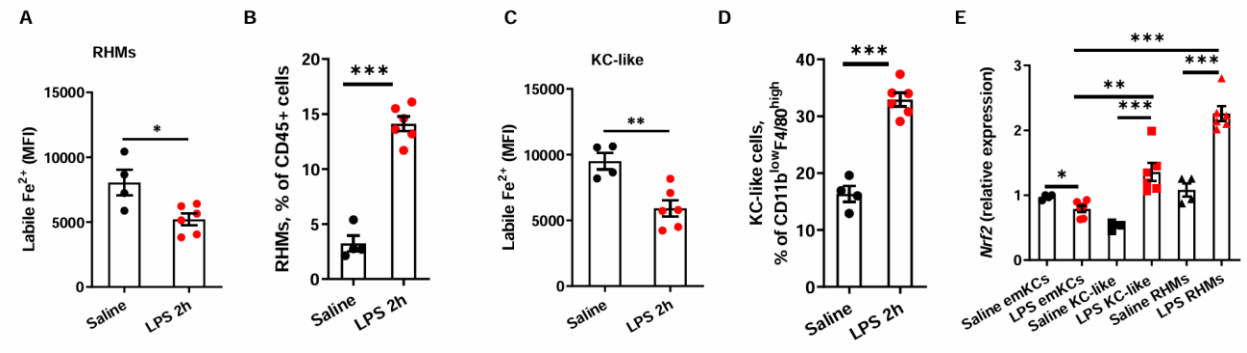


Figure 10: Iron phenotypes in RHMs and KC-like cells in response to LPS. The population and labile iron pool of KC-like cells (A&C; Tim4^{-}CD11b^{low}F4/80^{high}) and RHMs (B&D; CD11b^{high}F4/80^{low}) in NCD WT mice after 2 hours tail-vein injection of LPS. (E) *Nrf2* abundance in hepatic macrophages after LPS injection. Data are presented as mean ± SEM. *P < 0.05, **P < 0.01, ***P < 0.001, Student's t-test.

MyD88 signaling activation mediates iron metabolism-related gene expression in emKCs.

TLR/MyD88 is a well-established pathway induced by LPS in macrophages[34, 35]. To evaluate the impact of MyD88-related signaling on the expression of key genes associated with iron metabolism, 12wks old NCD LysMCre^{+}MyD88$^{f/f}$ vs. Cre^{-}MyD88$^{f/f}$ mice were tail-vein

injected with LPS (**Figure 11A**). After 2 hours, emKCs sorted from LPS-treated LysMCre^{+}MyD88$^{f/f}$mice had greater *Ncoa4* expression but less *Fth1* abundance (**Figures 11B&C**). In addition, LysMCre^{+}MyD88$^{f/f}$mice contained more emKCs than Cre^{-}MyD88$^{f/f}$ mice after 2 hours of LPS injection (**Figure 11D**). In NCD Cre^{-}MyD88$^{f/f}$ mice, we found that RHMs expressed about 3-fold greater MyD88 than emKCs (**Figure 11A**). In normal chow diet (NCD)-fed LysMCre^{+}MyD88$^{f/f}$ mice, MyD88 was also efficiently depleted in RHMs (**Figure 11A**). However, MyD88 depletion had minimal effects on RHM population and the expression of proinflammatory genes and iron metabolism genes (**Figures 11E-I**). Thus, these data suggest that MyD88-mediated signaling cascades mediates the expression of *Fth1* and *Ncoa4* in emKCs.

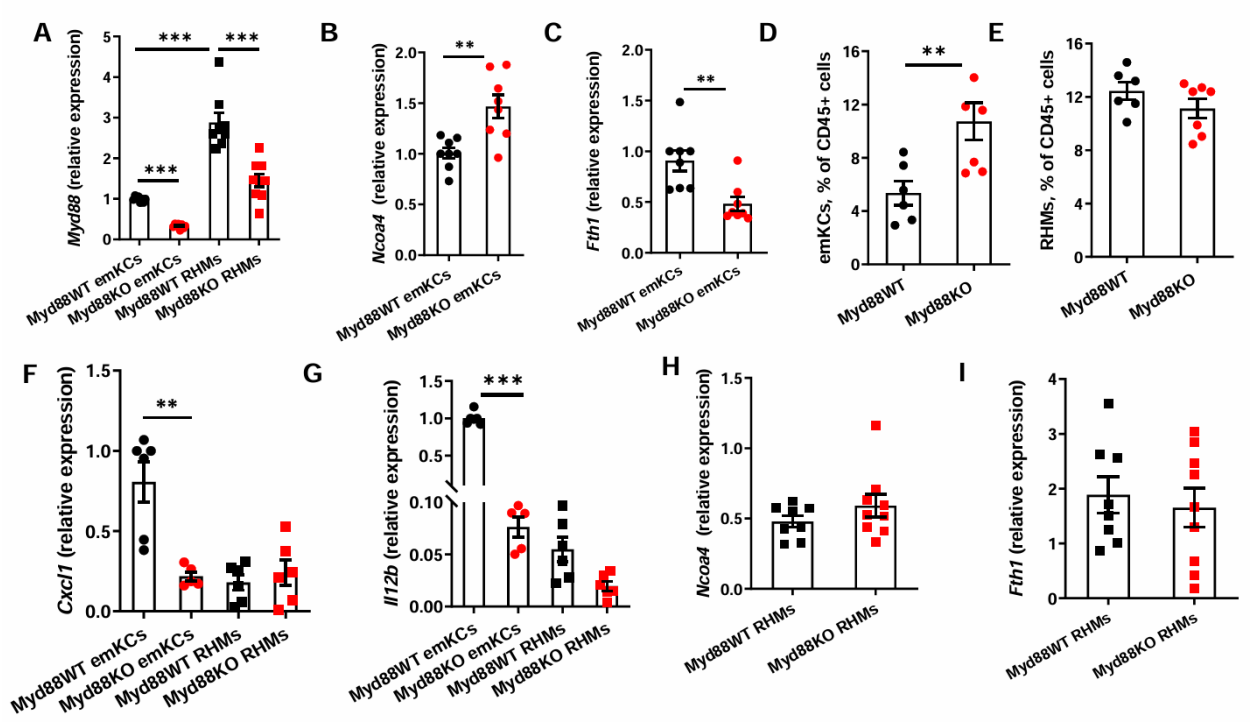


Figure 11: Effect of MyD88 depletion on the proinflammatory responses of emKCs and RHMs. (A) MyD88 abundance in emKCs and RHMs isolated from LysMcre^{+}MyD88$^{f/f}$ vs. Cre^{-}MyD8$^{f/f}$. After 2 hours tail-vein injection of LPS, *Ncoa4* and *Fth1* abundance in emKCs isolated from lean LysMcre^{+}MyD88$^{f/f}$ vs. Cre^{-}MyD8$^{f/f}$ (B-C). emKC and RHM population (D-E) and proinflammatory gene abundance (F-G) in lean LysMcre^{+}MyD88$^{f/f}$ vs. Cre^{-}MyD8$^{f/f}$ after 2 hours LPS injection. Effect of MyD88KO on *Ncoa4* and *Fth1* abundance of RHMs in response to LPS (H-I). Data are presented as mean ± SEM. *$P < 0.05$, ***$P < 0.001$, Student's t-test.

Ferritin depletion attenuates LPS-induced emKC abnormalities.

emKCs showed an increase in iron storing protein *Fth1* abundance in response to LPS injection, indicating LPS-induced iron overload in emKCs. We next evaluated the emKC phenotypes in KC-specific *Fth1* depletion mice (Clec4fCre^{+}/Fth1$^{f/f}$; **Figure 12A**)[36, 37]. While emKC population were comparable between Clec4fCre^{+}/Fth1$^{f/f}$ and Fth1$^{f/f}$ mice without LPS treatment, Clec4fCre^{+}/Fth1$^{f/f}$ mice contained more emKCs than Fth1$^{f/f}$ mice after 2 hours of LPS injection (**Figures 12B&C**). We also found that *Fth1* depletion attenuated the LPS-induced reduction in labile iron pool in emKCs (**Figure 12D**). KC-specific *Fth1* knockout had minimal effects on the population of KC-like cells and RHMs in LPS-injected mice (**Figures 12E&F**). In addition, *Fth1* knockout attenuated the LPS-induced production of *Tnfa* and *Cxcl1* but did not affect the expression of *Il12b* and *Il1b* in emKCs (**Figures 12G-J**). The levels of proinflammatory cytokines were comparable in RHMs between Clec4fCre^{+}/Fth1$^{f/f}$ and Fth1$^{f/f}$ mice after 2 hours of LPS injection (**Figures 12G-J**).

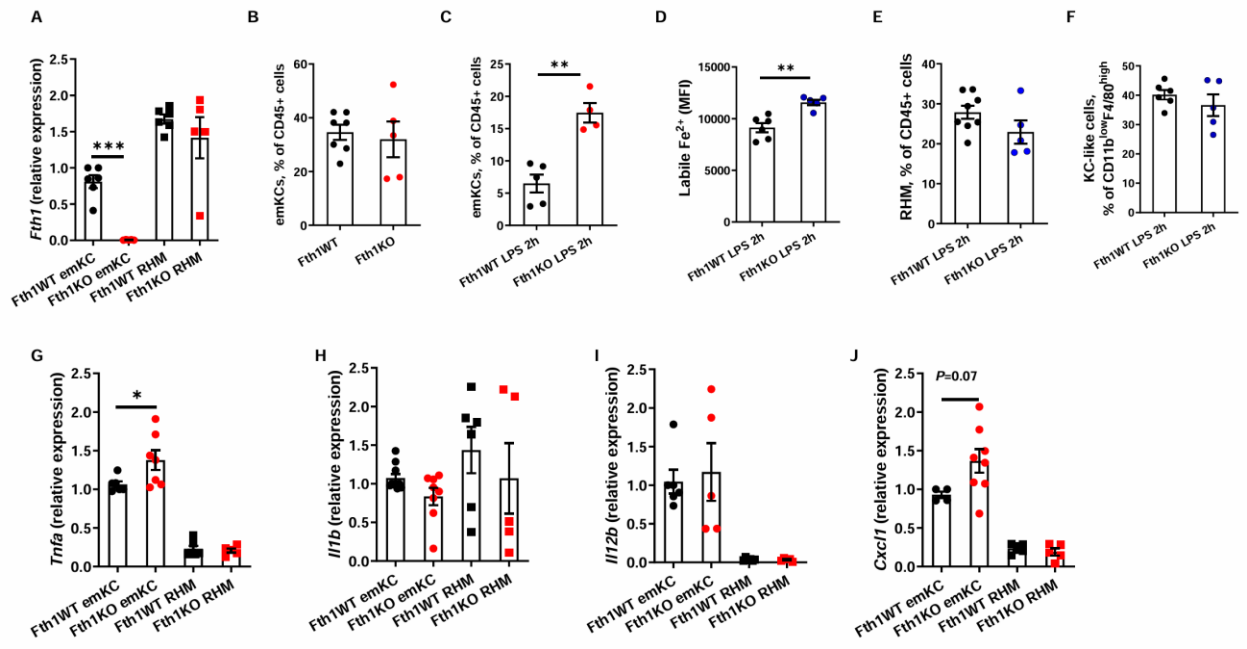


Figure 12: Effects of Fth knockout on emKC phenotypes in response to LPS. (A) *Fth1* abundance in emKCs and RHMs isolated from 10-12wks old male $Fth1^{f/f}$ (Fth1WT) or $Clec4fCre^{+}Fth1^{f/f}$ (Fth1KO) mice. The emKC population in Fth1WT or Fth1KO mice without (B) or with (C) LPS injection. The emKC labile iron pool (D), RHM (E) and KC-like cell (F) population in Fth1WT or Fth1KO after 2 hours of LPS injection. Proinflammatory cytokine abundance in emKCs and RHMs isolated from Fth1WT or Fth1KO after 2 hours of LPS injection (G-J). Data are presented as mean ± SEM. $*P < 0.05$, $**P < 0.01$, $***P < 0.001$, Student's t-test.

Iron phenotypes in hepatic macrophages post-infection.

We also assessed whether hepatic macrophages would be normalized after LPS injection. 2wks after one injection of LPS, emKC population was still less than that in the saline-injected control mice (**Figure 13A**). However, the RHM proportion was comparable among all mice after 2wks of LPS or saline injection (**Figure 13B**). The LPS-induced reduction in the abundance of *Ncoa4* and labile iron pool in emKCs still persisted 2 weeks after LPS injection (**Figures 13C&D**). However, the expression of proinflammatory cytokine Tnfa and other iron metabolism key genes were comparable among all mice 2 weeks after injection of either LPS or saline (**Figures 13E-H**)

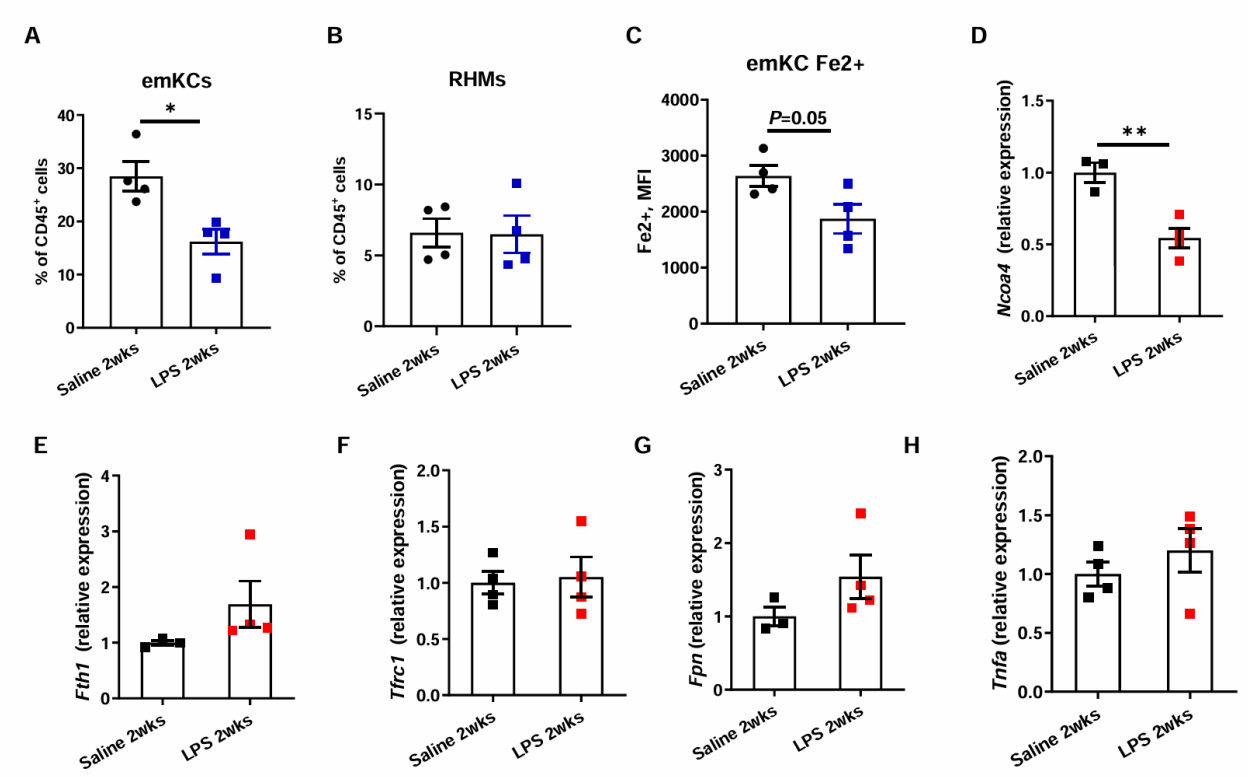


Figure 13: emKC phenotypes after 2 weeks of LPS injection. The population of emKCs (A) and RHMs (B) 2 weeks after one injection of LPS or saline. The levels of labile iron pool (C), *Ncoa4* (D), *Fth1* (E), *Tfrc1* (F), *Fpn* (G), *Tnfa* (H) in emKCs 2 weeks after one injection of LPS or saline. Data are presented as mean ± SEM. **P* < 0.05, ***P* < 0.01, Student's t-test.

Chapter 2 DISCUSSION

This study demonstrated that the change in iron homeostasis plays a critical role in triggering proinflammatory responses through controlling the influx of labile iron from labile iron pool into the mitochondria in macrophages. In the *in vitro* experiments, BMDMs exhibited iron deficiency and tuned down iron metabolism when challenged with LPS, but not in response to anti-inflammatory activation. In contrast, mitochondrial Fe^{2+} content was significantly increased in the presence of LPS. Supplying iron promotes LPS-induced proinflammatory responses in BMDMs. In the *in vivo* experiments with tail-vein injection of LPS, emKCs also quickly tune down the iron metabolism, whereas iron overload occurs in these macrophages. While LPS treatment does not affect BMDM survival, emKCs undergo a rapid loss in cell population after LPS challenging. Consistent with BMDMs, more labile iron is flowed into mitochondrial complex in emKCs in response to LPS. When mutating ferritin, more emKCs survive after LPS treatment, accompanied with elevated proinflammatory cytokine production. While LPS induces iron overload in KC-like cells and RHMs, these macrophage numbers are increased in response to LPS. In addition, LPS-treated KC-like cells and RHMs elevate the expression of NRF2, a master regulator of redox homeostasis, whereas NRF2 is repressed in emKCs after LPS treatment. 2 weeks after LPS challenging, emKCs are partially restored, demonstrating normalization in iron homeostasis and proinflammatory cytokine production.

Emerging evidence indicates that rapidly adjusting metabolism status exerts profound effects on the acute activation of macrophages. For example, TLR4 activation in BMDMs quickly leads to a transient change in metabolic state which boots up glycolysis and tricarboxylic acid cycle volume to elevate acetyl-Coenzyme A production which promotes histone acetylation[3]. Consistent with this rapid change in mitochondrial activities during

proinflammatory activation, we observed an increase in mitochondrial Fe^{2+} content in BMDMs after 2 hours of LPS stimulation. This LPS-induced increased level of labile iron influx into mitochondria also resulted in iron deficiency in BMDMs. When replenishing iron with FAC, LPS-induced proinflammatory responses were tuned up. However, in our studies, iron chelator DFO treatment had minimal effects on LPS-induced proinflammatory responses. Previous studies reported that DFO has low membrane permeability, especially barely entering mitochondria[26]. Indeed, the mitochondrial Fe^{2+} content of BMDMs was not affected by DFO treatment. An early study by Pereira et al. has shown that iron deprivation, especially in mitochondria, attenuates inflammation of human macrophages[26].

While NCOA4 has been demonstrated to be an important regulator of intracellular labile iron content in hepatocytes[38, 39], depletion of Ncoa4 did not significantly affect labile iron content in BMDMs. We also observed an increase in iron importer *Tfrc1* in BMDMs after mutating Ncoa4, probably acting as a compensatory pathway to maintain labile iron homeostasis.

emKCs are also one of iron-enriched cells[40, 41]. Similar to BMDMs, LPS induced a rapid repression on iron metabolism and a surge in mitochondrial Fe^{2+} content in emKCs. However, in contrast to iron deficiency in LPS-treated BMDMs, emKCs were characterized by iron overload after LPS tail-vein injection. LPS-induced iron overload was accompanied by a quick loss of emKC population, which is consistent with the observation from iron overload macrophages in previous studies[42, 43]. In contrast, in the mice with KC-specific mutation of iron storing protein ferritin, emKC loss was attenuated when challenging LPS. In addition, *Fth*1 knockout yielded greater levels of labile iron in emKCs, contributing to more mitochondrial Fe^{2+} content to elevate proinflammatory cytokine production.

In addition to emKCs, KC-like cells and RHMs exhibited iron overload in mice injected with LPS. However, the population of these hepatic macrophages was markedly increased in response to LPS injection. We noticed that NRF2, which is important to resolve ROS-induced abnormalities, was significantly elevated in both KC-like cells and RHMs when challenging LPS. In contrast, LPS caused a repression on NRF2 abundance in emKCs. These distinct NRF2 expression patterns may lead to the difference in the survival of these three types of hepatic macrophages. While emKC proportion greatly reduces in the presence of LPS, emKCs produce greater levels of proinflammatory cytokines than RHMs.

In response to LPS, MyD88-mediated signaling cascades serve as a critical part of TLR4 activation and modulate the activation of transcription factors and chromatin-modifying enzymes[44]. In macrophage-specific MyD88 knockout mice, the LPS-induced changes in iron metabolism key genes such as *Fth1* and *Ncoa4* were partially blocked, also attenuating LPS-induced emKC loss and proinflammatory responses. Interestingly, RHMs expressed about 3-fold more MyD88 than emKCs, whereas, MyD88 mutation had minimal effects on RHM phenotypes in response to LPS stimulation. Iron availability also regulates gene expression through affecting interaction between RNA-binding proteins and iron-responsive elements of genes[4, 45].

When resolving inflammation, emKC iron phenotypes were normalized but emKC population was still not fully recovered after 2 weeks of LPS injection. It is possible that emKC number would be fully restored after a longer time.

In summary, our findings highlight the significance of labile iron influx from labile iron pool to mitochondria to initiate proinflammatory activation of macrophages. Building upon our investigation into the iron metabolism during macrophage activation, the abnormalities on this labile iron influx could be pathogenic factors of macrophage inflammatory disorders

MATERIALS AND METHODS

Mouse models

To generate macrophage-specific MyD88 depletion mice, LysMCre mice were crossbred with MyD88 flox/flox (MyD88$^{f/f}$) mice to generate LysMCre^{+}MyD88$^{f/f}$ and Cre^{-}MyD88$^{f/f}$ mice. For Fth1 KO experiments, Clec4fCre^{+}/Fth1$^{f/f}$ and Fth1$^{f/f}$ mice were yielded by crossbreeding Clec4fCre and Fth1$^{f/f}$ mice. For *in vivo* experiments, only 10-12wks old male mice were used. All mice used in this study were male and maintained at 22°C in a 12/12-h light/dark cycle in a specific pathogen-free facility and given free access to food and water. All animal procedures were done in accordance with University of California, San Diego Research Guidelines for the Care and Use of Laboratory Animals and all animals were randomly assigned to cohorts when used.

LPS injection

Mice were treated with LPS (100ng/g of body weight) via tail vein injection. Livers from mice were harvested 2 hours after LPS injection.

Liver perfusion

To isolate non-parenchymal cells, liver was perfused through vena cava with 37°C warmed 50 mL of calcium and magnesium-free HBSS containing 10 mM HEPES and 0.25 mM EGTA, followed with 37°C warmed 30 mL of calcium and magnesium-contained HBSS with 10 mM HEPES, 0.1 mg/mL DNase I, and 0.75 mg/mL collagenase D. Then tissue was harvested, mashed in PBS containing 2% FBS, and filtered through 100 μm cell strainers. To remove liver parenchymal cells, 5-minute 50 x g, 80 x g, 100 x g, subsequent centrifugations were performed with supernatants followed by a 10-minute 1000 x g centrifugation to pellet the cells. Non-parenchymal cells were further purified using a 28% OptiPrep containing cells (lower)/PBS containing 2% FBS (upper) gradient centrifugation (1400 x g, 25 min, low acceleration, and no

brake at 4°C). The interphase was collected and red blood cells were lysed using 1X RBC Lysis Buffer.

BMDM differentiation and LPS or IL4/IL13 treatment

BMDMs prepared from 10-12wks old male or female B6/C57 WT mice. Bone marrow was extracted from mice leg bones and collected in PBS containing 2% FBS. 5-minute 500 x g centrifugation was performed and red blood cells were lysed with 1X RBC Lysis Buffer. Cells were cultured in DMEM complete medium (1X DMEM, 10% FBS, 100X Pen strep, 100X Glutamax) with 10ng/ml M-CSF. For M1 differentiation: After 7 days, media was replaced with 10ng/ml LPS in DMEM complete medium and cultured for 24 hours. For M2 differentiation: After 7 days, media was replaced with 20ng/ml IL-4 and 20ng/ml IL-13 in DMEM complete medium and cultured for 24 hours.

FAC or DFO treatment in BMDMs

BMDMs were cultured and differentiated with M-CSF as described above for 7 days. Then, media was replaced with 100nM FAC or DFO in DMEM complete medium and cultured for 24 hours.

siRNA transfection

BMDMs were cultured and differentiated with M-CSF as described above for 7 days. Cells were treated with 1.5ul (scramble mimic or Ncoa4) + 3ul RNAi MAX + 50ul OptiMEM per 1ml DMEM complete medium per well. Media was replaced with DMEM complete medium 8 hours after transfection.

Flow cytometric assay and markers of macrophages.

For cell surface molecules staining, single cell suspension in HBSS was Fc receptor-blocked with purified anti-mouse CD16/32 antibody at room temperature for 5 min and further stained with antibodies: Tim4, F4/80, CD11b, CD45, MHCII, MitoFerro Green, MitoSOX Red. MitoTracker Deep Red, with LIVE/DEAD™ Fixable Aqua Dead Cell dye at room temperature

for 40 min. Flow cytometry analysis and cell sorting were performed using the MA900 sorter (SONY). Data were analyzed using FlowJo. Embryonic Kupffer cells were gated on Tim4^{+}CD11b^{low}F4/80^{high}; Kupffer-like cells were gated on Tim4^{-} CD11b^{low}F4/80^{high}; recruited hepatic macrophage were gated on CD11b^{high}F4/80^{low}. These populations were collected into Trizol for further RNA extraction.

Labile iron measurements

A fluorescent probe BioTracker Far-red Labile Fe2+ Dye was used in flow cytometric analysis to characterize ER-bound labile iron (Fe2+). Cells were stained with this probe as described above.

Mitochondrial phenotype evaluation

Fluorescent probes for flow cytometry were used to characterize different parts of the mitochondrial phenotype. MitoFerro Green was used as a probe for mitochondrial Fe2+. Mitochondrial mass was measured by MitoTrack Green. Mitochondrial ROS was measured by MitoSOX Red. Fluorescent probes were stained as described above.

RNA extraction and qPCR

RNA was isolated using TRIzol reagent (Invitrogen) according to the manufacturer's instructions. 10 μg of glycogen (RNA grade) was added to help RNA precipitation. Complementary DNA was synthesized using High-Capacity cDNA Reverse Transcription Kit. qPCR was performed using PerfeCTa SYBR Green FastMix (Quantabio) on a QuantStudio™ 3 Real-Time PCR Instrument (Thermo Fisher Scientific). Quantification of relative expression was normalized to β-actin.

Quantification and statistical analysis.

Blinding was performed whenever deemed to be appropriate and applicable. Sample description and identification was unavailable to the core personnel during data plotting and analyses. No samples or data were excluded from the study for statistical purposes. Each *in vitro*

experiment was independently performed in duplicate or triplicate to ensure reproducibility. Group sizes of 5 mice or greater were sufficient to reach a statistical power of at least 80%. Mice were assigned at random to treatment groups for all mouse studies. Tests used for statistical analyses are described in the figure legends. To assess whether the means of two groups are statistically different from each other, unpaired two-tailed Student's *t*-test was used for statistical analyses, all data passed the normality test using Prism8 software (GraphPad software v8.0; Prism, La Jolla, CA). *P* values of 0.05 or less were considered to be statistically significant. Degrees of significance are indicated in the figure legends.

REFERENCES

1. Nonnenmacher Y and Hiller K. Biochemistry of proinflammatory macrophage activation. *Cell Mol Life Sci*. 2018;75:2093-2109.

2. Faas M, Ipseiz N, Ackermann J, Culemann S, Grüneboom A, Schröder F, Rothe T, Scholtysek C, Eberhardt M, Böttcher M, Kirchner P, Stoll C, Ekici A, Fuchs M, Kunz M, Weigmann B, Wirtz S, Lang R, Hofmann J, Vera J, Voehringer D, Michelucci A, Mougiakakos D, Uderhardt S, Schett G and Krönke G. IL-33-induced metabolic reprogramming controls the differentiation of alternatively activated macrophages and the resolution of inflammation. *Immunity*. 2021;54:2531-+.

3. Lauterbach MA, Hanke JE, Serefidou M, Mangan MSJ, Kolbe CC, Hess T, Rothe M, Kaiser R, Hoss F, Gehlen J, Engels G, Kreutzenbeck M, Schmidt SV, Christ A, Imhof A, Hiller K and Latz E. Toll-like Receptor Signaling Rewires Macrophage Metabolism and Promotes Histone Acetylation via ATP-Citrate Lyase. *Immunity*. 2019;51:997-1011 e7.

4. Muckenthaler MU, Rivella S, Hentze MW and Galy B. A Red Carpet for Iron Metabolism. *Cell*. 2017;168:344-361.

5. Harrison PM and Arosio P. The ferritins: molecular properties, iron storage function and cellular regulation. *Biochim Biophys Acta*. 1996;1275:161-203.

6. Dowdle WE, Nyfeler B, Nagel J, Elling RA, Liu S, Triantafellow E, Menon S, Wang Z, Honda A, Pardee G, Cantwell J, Luu C, Cornella-Taracido I, Harrington E, Fekkes P, Lei H, Fang Q, Digan ME, Burdick D, Powers AF, Helliwell SB, D'Aquin S, Bastien J, Wang H, Wiederschain D, Kuerth J, Bergman P, Schwalb D, Thomas J, Ugwonali S, Harbinski F, Tallarico J, Wilson CJ, Myer VE, Porter JA, Bussiere DE, Finan PM, Labow MA, Mao X, Hamann LG, Manning BD, Valdez RA, Nicholson T, Schirle M, Knapp MS, Keaney EP and Murphy LO. Selective VPS34 inhibitor blocks autophagy and uncovers a role for NCOA4 in ferritin degradation and iron homeostasis in vivo. *Nat Cell Biol*. 2014;16:1069-79.

7. Mancias JD, Wang X, Gygi SP, Harper JW and Kimmelman AC. Quantitative proteomics identifies NCOA4 as the cargo receptor mediating ferritinophagy. *Nature*. 2014;509:105-9.

8. Mancias JD, Pontano Vaites L, Nissim S, Biancur DE, Kim AJ, Wang X, Liu Y, Goessling W, Kimmelman AC and Harper JW. Ferritinophagy via NCOA4 is required for erythropoiesis and is regulated by iron dependent HERC2-mediated proteolysis. *Elife*. 2015;4.

9. Soares MP and Hamza I. Macrophages and Iron Metabolism. *Immunity*. 2016;44:492-504.

10. Abboud S and Haile DJ. A novel mammalian iron-regulated protein involved in intracellular iron metabolism. *J Biol Chem*. 2000;275:19906-12.

11. Donovan A, Brownlie A, Zhou Y, Shepard J, Pratt SJ, Moynihan J, Paw BH, Drejer A, Barut B, Zapata A, Law TC, Brugnara C, Lux SE, Pinkus GS, Pinkus JL, Kingsley PD, Palis J, Fleming MD, Andrews NC and Zon LI. Positional cloning of zebrafish ferroportin1 identifies a conserved vertebrate iron exporter. *Nature*. 2000;403:776-81.

12. McKie AT, Marciani P, Rolfs A, Brennan K, Wehr K, Barrow D, Miret S, Bomford A, Peters TJ, Farzaneh F, Hediger MA, Hentze MW and Simpson RJ. A novel duodenal iron-regulated transporter, IREG1, implicated in the basolateral transfer of iron to the circulation. *Mol Cell*. 2000;5:299-309.

13. Pereira M, Chen TD, Buang N, Olona A, Ko JH, Prendecki M, Costa ASH, Nikitopoulou E, Tronci L, Pusey CD, Cook HT, McAdoo SP, Frezza C and Behmoaras J. Acute Iron Deprivation Reprograms Human Macrophage Metabolism and Reduces Inflammation. *Cell Rep*. 2019;28:498-+.

14. Gillen KM, Mubarak M, Nguyen TD and Pitt D. Significance and In Vivo Detection of Iron-Laden Microglia in White Matter Multiple Sclerosis Lesions. *Front Immunol*. 2018;9:255.

15. Vinchi F, Costa da Silva M, Ingoglia G, Petrillo S, Brinkman N, Zuercher A, Cerwenka A, Tolosano E and Muckenthaler MU. Hemopexin therapy reverts heme-induced proinflammatory phenotypic switching of macrophages in a mouse model of sickle cell disease. *Blood*. 2016;127:473-86.

16. Nandal A, Ruiz JC, Subramanian P, Ghimire-Rijal S, Sinnamon RA, Stemmler TL, Bruick RK and Philpott CC. Activation of the HIF prolyl hydroxylase by the iron chaperones PCBP1 and PCBP2. *Cell Metab*. 2011;14:647-57.

17. Frey AG, Nandal A, Park JH, Smith PM, Yabe T, Ryu MS, Ghosh MC, Lee J, Rouault TA, Park MH and Philpott CC. Iron chaperones PCBP1 and PCBP2 mediate the metallation of the dinuclear iron enzyme deoxyhypusine hydroxylase. *Proc Natl Acad Sci U S A*. 2014;111:8031-6.

18. Hamdi A, Roshan TM, Kahawita TM, Mason AB, Sheftel AD and Ponka P. Erythroid cell mitochondria receive endosomal iron by a "kiss-and-run" mechanism. *Biochim Biophys Acta*. 2016;1863:2859-2867.

19. Luo Z, Ji Y, Gao H, Gomes Dos Reis FC, Bandyopadhyay G, Jin Z, Ly C, Chang YJ, Zhang D, Kumar D and Ying W. CRIg(+) Macrophages Prevent Gut Microbial DNA-Containing Extracellular Vesicle-Induced Tissue Inflammation and Insulin Resistance. *Gastroenterology*. 2021;160:863-874.

20. Luo Z, Ji Y, Zhang D, Gao H, Jin Z, Yang M and Ying W. Microbial DNA enrichment promotes liver steatosis and fibrosis in the course of non-alcoholic steatohepatitis. *Acta Physiol (Oxf)*. 2022;235:e13827.

21. Ying W, Cheruku PS, Bazer FW, Safe SH and Zhou B. Investigation of macrophage polarization using bone marrow derived macrophages. *J Vis Exp*. 2013.

22. Asada-Senju M, Maeda T, Sakata T, Hayashi A and Suzuki T. Molecular analysis of the transferrin gene in a patient with hereditary hypotransferrinemia. *J Hum Genet*. 2002;47:355-9.

23. Tong AJ, Liu X, Thomas BJ, Lissner MM, Baker MR, Senagolage MD, Allred AL, Barish GD and Smale ST. A Stringent Systems Approach Uncovers Gene-Specific Mechanisms Regulating Inflammation. *Cell*. 2016;165:165-179.

24. Hirayama T, Tsuboi H, Niwa M, Miki A, Kadota S, Ikeshita Y, Okuda K and Nagasawa H. A universal fluorogenic switch for Fe(ii) ion based on N-oxide chemistry permits the visualization of intracellular redox equilibrium shift towards labile iron in hypoxic tumor cells. *Chem Sci*. 2017;8:4858-4866.

25. Ballas SK, Zeidan AM, Duong VH, DeVeaux M and Heeney MM. The effect of iron chelation therapy on overall survival in sickle cell disease and beta-thalassemia: A systematic review. *Am J Hematol*. 2018;93:943-952.

26. Pereira M, Chen TD, Buang N, Olona A, Ko JH, Prendecki M, Costa ASH, Nikitopoulou E, Tronci L, Pusey CD, Cook HT, McAdoo SP, Frezza C and Behmoaras J. Acute Iron Deprivation Reprograms Human Macrophage Metabolism and Reduces Inflammation In Vivo. *Cell Rep*. 2019;28:498-511 e5.

27. Hirayama T, Kadota S, Niwa M and Nagasawa H. A mitochondria-targeted fluorescent probe for selective detection of mitochondrial labile Fe(ii). *Metallomics*. 2018;10:794-801.
28. Zhou R, Yazdi AS, Menu P and Tschopp J. A role for mitochondria in NLRP3 inflammasome activation. *Nature*. 2011;469:221-5.

29. Kauffman ME, Kauffman MK, Traore K, Zhu H, Trush MA, Jia Z and Li YR. MitoSOX-Based Flow Cytometry for Detecting Mitochondrial ROS. *React Oxyg Species (Apex)*. 2016;2:361-370.

30. Tilg H, Zmora N, Adolph TE and Elinav E. The intestinal microbiota fuelling metabolic inflammation. *Nat Rev Immunol*. 2020;20:40-54.

31. Seidman JS, Troutman TD, Sakai M, Gola A, Spann NJ, Bennett H, Bruni CM, Ouyang Z, Li RZ and Sun X. Niche-specific reprogramming of epigenetic landscapes drives myeloid cell diversity in nonalcoholic steatohepatitis. *Immunity*. 2020;52:1057-1074.

32. Yamamoto M, Kensler TW and Motohashi H. The KEAP1-NRF2 System: a Thiol-Based Sensor-Effector Apparatus for Maintaining Redox Homeostasis. *Physiol Rev*. 2018;98:1169-1203.

33. Nguyen T, Nioi P and Pickett CB. The Nrf2-antioxidant response element signaling pathway and its activation by oxidative stress. *J Biol Chem*. 2009;284:13291-5.

34. Palsson-McDermott EM and O'Neill LA. Signal transduction by the lipopolysaccharide receptor, Toll-like receptor-4. *Immunology*. 2004;113:153-62.

35. Chow JC, Young DW, Golenbock DT, Christ WJ and Gusovsky F. Toll-like receptor-4 mediates lipopolysaccharide-induced signal transduction. *J Biol Chem*. 1999;274:10689-92.

36. Sakai M, Troutman TD, Seidman JS, Ouyang Z, Spann NJ, Abe Y, Ego KM, Bruni CM, Deng Z, Schlachetzki JCM, Nott A, Bennett H, Chang J, Vu BT, Pasillas MP, Link VM, Texari L, Heinz S, Thompson BM, McDonald JG, Geissmann F and Glass CK. Liver-Derived Signals Sequentially Reprogram Myeloid Enhancers to Initiate and Maintain Kupffer Cell Identity. *Immunity*. 2019;51:655-670 e8.

37. Darshan D, Vanoaica L, Richman L, Beermann F and Kuhn LC. Conditional deletion of ferritin H in mice induces loss of iron storage and liver damage. *Hepatology*. 2009;50:852-60.

38. Li XQ, Lozovatsky L, Sukumaran A, Gonzalez L, Jain A, Liu D, Ayala-Lopez N and Finberg KE. is regulated by HIF and mediates mobilization of murine hepatic iron stores after blood loss. *Blood*. 2020;136:2691-2702.

39. Bellelli R, Federico G, Matte A, Colecchia D, Iolascon A, Chiariello M, Santoro M, De Franceschi L and Carlomagno F. NCOA4 Deficiency Impairs Systemic Iron Homeostasis. *Cell Rep*. 2016;14:411-421.

40. Nairz M, Theurl I, Swirski FK and Weiss G. "Pumping iron"-how macrophages handle iron at the systemic, microenvironmental, and cellular levels. *Pflugers Arch*. 2017;469:397-418.

41. Scott CL and Guilliams M. The role of Kupffer cells in hepatic iron and lipid metabolism. *J Hepatol*. 2018;69:1197-1199.

42. Andrianaki AM, Kyrmizi I, Thanopoulou K, Baldin C, Drakos E, Soliman SSM, Shetty AC, McCracken C, Akoumianaki T, Stylianou K, Ioannou P, Pontikoglou C, Papadaki HA, Tzardi M, Belle V, Etienne E, Beauvais A, Samonis G, Kontoyiannis DP, Andreakos E, Bruno VM, Ibrahim AS and Chamilos G. Iron restriction inside macrophages regulates pulmonary host defense against Rhizopus species. *Nat Commun*. 2018;9:3333.

43. Cai J, Zhang M, Liu Y, Li H, Shang L, Xu T, Chen Z, Wang F, Qiao T and Li K. Iron accumulation in macrophages promotes the formation of foam cells and development of atherosclerosis. *Cell Biosci*. 2020;10:137.

44. Kawai T and Akira S. The role of pattern-recognition receptors in innate immunity: update on Toll-like receptors. *Nat Immunol*. 2010;11:373-84.

45. Wilkinson N and Pantopoulos K. The IRP/IRE system in vivo: insights from mouse models. *Front Pharmacol*. 2014;5:176.